Volatile distributions in and on the Moon revealed by Cu and Fe isotopes in the 'Rusty Rock' 66095

James M.D. Day, Paolo Sossi, Charles Shearer, Frédéric Moynier

HAL Id: insu-02916838
https://insu.hal.science/insu-02916838

1   **Volatile distributions in and on the Moon revealed by Cu and**

2   **Fe isotopes in the 'Rusty Rock' 66095**

3

4

5   James M.D. Day[1,2*], Paolo A. Sossi[2], Charles K. Shearer[3], Frederic Moynier[2,4]

6

7   [1]Scripps Institution of Oceanography, University of California San Diego, La Jolla, CA
8   92093-0244, USA
9   [2]Institut de Physique du Globe de Paris, Université Paris Diderot, Sorbonne Paris Cité, 1
10   rue Jussieu, 75005, Paris, France
11   [3]Institute of Meteoritics, University of New Mexico, Albuquerque, NM 87131, USA
12   [4]Institut Universitaire de France, 75005, Paris
13

14   *Corresponding author: jmdday@ucsd.edu

15

16

19

20

21

22   Abstract Length: 381

23   Total word count: 6548

24   Figures: 5

25   Tables: 2

26

27

28

29

30
31
32
33

36 **ABSTRACT**

37 The Apollo 16 'Rusty Rock' impact melt breccia 66095 is a volatile-rich sample, with the

38 volatiles inherited through vapor condensation from an internal lunar source formed

39 during thermo-magmatic evolution of the Moon. We report Cu and Fe isotope data for

40 66095 and find that bulk-rocks, residues and acid leaches span a relatively limited range

41 of compositions (3.0 ±1.3 wt.% FeO [range = 2.0-4.8 wt.%], 5.4 ±3.1 ppm Cu [range = 3-

42 12 ppm], average δ^{56}Fe of 0.15 ± 0.05‰ [weighted mean = 0.16‰] and δ^{65}Cu of 0.72 ±

43 0.14‰ [weighted mean = 0.78‰]). In contrast to the extreme enrichment of light

44 isotopes of Zn and heavy isotopes of Cl in 66095, δ^{65}Cu and δ^{56}Fe in the sample lie

45 within the previously reported range for lunar mare basalts (0.92 ± 0.16‰ and 0.12 ±

46 0.02‰, respectively). The lack of extreme isotopic fractionation for Cu and Fe isotopes

47 reflects compositions inherent to 66095, with condensation of a cooling gas from impact-

48 generated fumarolic activity at temperatures too low to lead to the condensation of Cu

49 and Fe, but higher than required to condense Zn. Together with thermodynamic models,

50 these constraints suggest that the gas condensed within 66095 between 700 and 900 °C

51 (assuming a pressure of 10^{-6} and an fO$_2$ of IW-2). That the Cu and Fe isotopic

52 compositions of sample 66095 are within the range of mare basalts removes the need for

53 an exotic, volatile-enriched source. The enrichment in Tl, Br, Cd, Sn, Zn, Pb, Rb, Cs, Ga,

54 B, Cl, Li relative to Bi, Se, Te, Ge, Cu, Ag, Sb, Mn, P, Cr and Fe in the 'Rusty Rock' is

55 consistent with volcanic outgassing models and indicates that 66095 likely formed distal

56 from the original source of the gas. The volatile-rich character of 66095 is consistent with

57 impact-generated fumarolic activity in the region of the Cayley Plains, demonstrating that

58 volatile-rich rocks can occur on the lunar surface from outgassing of a volatile-poor lunar

59 interior. The 'Rusty Rock' indicates that the lunar interior is significantly depleted in

60 volatile elements and compounds and that volatile-rich lunar surface rocks likely formed

61 through vapor condensation. Remote sensing studies have detected volatiles on the lunar

62 surface, attributing them dominantly to solar wind. Based on the 'Rusty Rock', some of

63 these surface volatiles may also originate from the Moon's interior.

1. Introduction

Knowledge of the origin and distribution of volatile elements in and on the Moon is important for models of Earth-Moon system formation and planetary accretion and differentiation, as well as for understanding volcanism and surface volatile distributions (e.g., Taylor, 2012; Day & Moynier, 2014). Initial work on Apollo samples found that the Moon is depleted with respect to the bulk silicate Earth for elements that are cosmochemically volatile or moderately volatile (e.g., Wolf & Anders, 1980; Jones & Palme, 2000). In this respect, volatile or moderately volatile elements can be defined by the 50% condensation temperatures at gas pressures of $<10^{-4}$ bar of 665 K and 1135 K, respectively (Lodders, 2003). Early measurements of low initial Rb/Sr and high U/Pb ratios for lunar rocks implied an interior devoid of volatile and moderately volatile elements since its inception (Papanastassiou et al., 1970; Tatsumoto & Rosholt, 1970). Stable isotope signatures of Zn (Paniello et al., 2012; Kato et al., 2015), K (Wang & Jacobsen, 2016), Cl (Sharp et al., 2010; Boyce et al. 2016), Cr (Sossi et al. 2018), Ga (Kato & Moynier, 2017) and Rb (Pringle & Moynier, 2017) indicate that evaporation/condensation processes during or following lunar formation control the depletion in these elements. Regardless of when volatile depletion occurred, extreme depletions of volatile elements in lunar rocks, compared with primitive meteorites and Earth, indicate a highly energetic formation process and catastrophic outgassing of the material that formed the Moon (Day & Moynier, 2014; Albarède et al., 2015).

In contrast to evidence for a volatile-depleted Moon, studies of some Apollo lunar crustal rocks have shown modest enrichment in moderately volatile elements (e.g., Krahenbuhl et al., 1973). Lunar pyroclastic glass beads have Pb compositions revealing a source with $^{238}U/^{204}Pb$ (~25) only four times more depleted than Earth's mantle ($^{238}U/^{204}Pb$ = ~6-8; Tatsumoto et al., 1987), while elevated abundances of OH, F, Cl and S in olivine melt inclusions from pyroclastic glass beads and mare basalts indicate that they are volatile-enriched (Hauri et al., 2011; Chen et al., 2014). Water appears to be more depleted in the Moon than in Earth, however. For example, there is no petrographic evidence for water-rich mineral phases such as amphibole in mare basalts, which may relate to their lack of stability (e.g., Sisson & Grove, 1993) due to low contents of

95   moderately volatile Na and K in mesostasis and bulk lunar igneous rocks. Isotopically

96   light Zn, Cu and Fe compositions also characterize the pyroclastic glasses (Moynier et al.,

97   2006; Herzog et al., 2009; Kato et al., 2015), as well as light Zn in some mare basalts and

98   crustal rocks (Paniello et al. 2012; Kato et al., 2015; Day et al., 2017), indicating volatile-

99   rich vapor condensation. These signatures are inconsistent with complete evaporative loss

100   of volatile elements from the Moon, requiring that some volatile components exist in its

101   interior.

102

103   It is now established that volatile deposits occur on the lunar surface. Data from

104   remote sensing missions have identified H-bearing species not only within permanently-

105   shadowed cold traps at polar regions, but also in non-polar regions of the Moon (e.g.

106   Feldman et al., 1998; Pieters et al., 2009; Paige et al., 2010; Colaprete et al., 2010; Li &

107   Milliken, 2017). While much of this volatile-rich material has been attributed to solar

108   wind implantation, some fraction of the volatile inventory may originate from lunar

109   interior sources, even if the interior source was initially volatile-depleted (Day et al.,

110   2017).

111

112   To examine the distribution of volatile elements in and on the Moon, we present

113   new Cu and Fe isotope data for the 'rusty rock', 66095. Sample 66095 is notable for

114   several reasons. First, it is a type-example of a volatile-enriched lunar sample, with

115   elevated contents of Bi, Br, Cd, Cl, Ge, I, Pb, Sb, Tl and Zn compared to other lunar

116   samples (Krahenbuhl et al., 1973; Wanke et al., 1981; Jovanovic & Reed, 1981; Ebihara

117   et al., 1992; Day et al., 2017). It is a fine to medium-grained impact melt breccia with

118   elevated highly siderophile element abundances (0.001-0.1 × CI Chondrite; Day et al.,

119   2017) that contains clasts of anorthosite, troctolite and basalt and an incompatible-

120   element rich ['KREEPy'] geochemical signature. Fragments of the impact melt breccia

121   define an ^{87}Rb-^{87}Sr formation age of 4.06 ±0.24 Ga that is identical, within uncertainty,

122   of the ^{207}Pb-^{206}Pb age of 4.01 ±0.06 Ga (Nunes & Tatsumoto, 1973). Initial ^{87}Sr/^{86}Sr for

123   66095 is 0.69909 ±5, consistent with a source with low long-term time-integrated Rb/Sr

124   (Day et al., 2017), while 85% of Pb in 66095 is unsupported by radioactive decay of U

125   and Th, requiring a high ^{238}U/^{204}Pb (>570) source (Nunes & Tatsumoto, 1973). Second,

126   the 'rusty' character of 66095 is due to the presence of akaganéite (FeOOH; Taylor et al.,

127   1973) and lawrencite (FeCl$_2$; Shearer et al., 2014). The presence of these minerals has led

128   to the hypothesis that volatile element enrichment occurred in 66095 either through

129   alteration during transit to Earth (Taylor et al., 1973), or through fumarolic activity on the

130   Moon (Krahenbuhl et al., 1973; Nunes & Matsumoto, 1973; Shearer et al., 2014). During

131   fumarolic activity, temperatures and Cl-rich gas compositions inferred for this process are

132   potentially sufficient to mobilize the moderately volatile elements in the vapor phase.

133   Both Fe and Cu tend to form chloro-complexes at low temperatures (<700 °C), whereas

134   the monatomic gas species are stable at magmatic temperatures (Renggli et al. 2017). The

135   stable isotopic fractionation between these different species and the condensed phase can

136   therefore be used to query the nature of vapor deposition observed in 66095. In this

137   study, we examine the isotopic and elemental fractionation of Cu and Fe with respect to

138   other volatile and moderately volatile elements, and the implications for volatiles both in

139   and on the Moon.

140

141   **2. Sample, leaching/etching and digestion procedures**

142   Three fragments of the 'Rusty Rock', 66095, 421 (163 mg), 66095, 425 (173 mg)

143   and 66095, 430 (201 mg) were used to measure Fe and Cu isotope compositions, with Zn

144   isotope data presented for the samples previously by Day et al. (2017). Samples 66095,

145   421 and 66095, 430 were dominantly grey crystalline material with no visible clasts,

146   similar to fragments of poikilitic impact melt described previously (Garrison & Taylor,

147   1980; Hunter & Taylor, 1981). Sample 66095, 425 was composed of pale-colored

148   anorthosite-rich material, with black vitrophyric impact-melt glass. This clast is like the

149   'cataclastic anorthosite' clasts noted by Garrison & Taylor (1980).

150

151   A goal in studying 66095 was to assess isotopic heterogeneity within fragments of

152   the sample, and a procedure of crushing and leaching/etching was designed and

153   performed on samples (Table S1 of Day et al., 2017). These protocols were developed

154   based on previous leaching experiments and observations of volatile element

155   heterogeneity observed in fragments of 66095 (Jovanovic and Reed, 1981). In the first

156   stage, sample 66095, 421 was powdered as a whole-rock sample, with no leaching or

157   modification. Samples 66095, 425 and 66095, 430 were broken into two fragments. One

158   fragment of each of these samples was powdered and digested, with no leaching or

159   modification. These samples make up the 'bulk' measurements given in **Table 1**. The

160   remaining materials, including powder from 66095, 421 and ground fragments from

161   66095, 425 and 66095, 430 were leached and the leachates (labelled as L) and residual

162   fragments (labelled as R) were dried and precisely weighed to calculate concentrations.

163   Drying was performed between each leaching or etching step and was done in a class-10

164   hood at 100˚C. Weighing was done at room temperature (21.5˚C) in Teflon vessels using

165   a Mettler Toledo XPE205 Analytical Balance with repeatability of 0.007 mg.

166

167   Three different leaching/etching experimental processes were used. For aliquots

168   of 66095, 425(B) and 66095, 430 the sample powder was leached for 30 minutes in 18.2

169   MΩ H_2O and the leachate was then separated from the residue (Exp. 1). For aliquots of

170   66095, 421 and 66095, 430, the sample powder was leached for 30 minutes in 1M HCl

171   and the leachate separated from the residue (Exp. 2). Finally, a three-step leaching

172   process was employed on 66095, 421 (Exp. 3). The first step was a 20-minute leach in

173   18.2 MΩ H_2O, with ultra-sonification at 30°C. The H_2O leachate was extracted, and 3M

174   HCl was then added to the residue after dry-down and weighing. This second step was

175   also for 20 minutes, with ultra-sonification at 30°C. When the 3M HCl was extracted

176   from the residue, a strong odor of H_2S was noticeable from all samples. The final etching

177   stage involved addition of 1M HF-HNO_3 after drying of the residue and weighing.

178   Reaction for this final stage took place for 2 hours on a hotplate at 60°C. After extraction

179   of this final leaching stage, samples were dried down, and weighed prior to treatment in

180   an identical fashion for dissolution, as described below. A total of 15 leachates/etchates,

181   residues and whole-rock powders were measured for Fe isotope compositions and

182   abundances, and 10 were analyzed for Cu isotope compositions due to limited available

183   Cu in some of the water leachates.

184

185   After leaching/etching, all samples were dissolved in a 4:1 mixture of ultra-pure

186   HF/HNO_3 in Teflon beakers for 96 hours, dried down and then dissolved and further

187 dried-down in 6M HCl twice to remove fluorides. Remaining solutions, after Zn column

188 chemistry, were used to obtain Cu and Fe isotopic compositions.

189

190 **3. Analytical protocols for Cu and Fe isotope analysis**

191 All samples and external standards were purified for Cu isotope analysis using a

192 single column ion chromatographic technique (modified after Maréchal et al., 1999 and

193 used in Sossi et al., 2015). The procedure utilizes Bio-Rad AG1-X8 anion exchange

194 resin, which, at low pH in chloride form, has a high partition coefficient for Cu. Sample

195 aliquots were loaded onto 1 mL of the AG1-X8 (200-400 mesh) resin on 0.4×7 cm

196 Teflon columns and matrix elements were eluted in 5 mL of 6 M HCl. The Cu was then

197 eluted in a further 10 ml of 6 M HCl. Iron was then eluted taken in 4 mL of 0.5 M HCl.

198 Samples were evaporated to dryness and the whole procedure was repeated to further

199 purify Cu and Fe. The final purified Cu and Fe fractions were taken up in 0.32 M HNO_3

200 and made up to 300 ppb and 2 ppm, respectively, and doped with 300 ppb and 5 ppm of

201 Ni, respectively, for analysis.

202

203 Copper isotope analysis was performed on a *ThermoScientific* Neptune Plus

204 Multi-Collector Inductively-Coupled-Plasma Mass-Spectrometer (MC-ICP-MS) at the

205 Institut de Physique du Globe, Paris. Samples were introduced into the instrument using

206 an ESI PFA microflow nebuliser (100 µl min^{-1} flow rate) running into a quartz spray

207 chamber following the procedure of Sossi et al. (2015). The instrument was operated at

208 low resolution (m/Δm ~ 450, where Δm is defined at 5 % and 95 % of peak height), with

209 the ^{65}Cu and ^{63}Cu beams collected in the C (central) and L2 Faraday cups respectively.

210 The Ni masses (^{60}Ni, ^{61}Ni, ^{62}Ni) were collected in cups L3, L2 and L1, respectively.

211 Under typical running conditions, a 300 ppb Cu solution generated a 0.06-0.08 nA ion

212 beam (6-8 V total signal using 10^{11} Ω resistors). To ensure sufficient counting statistics

213 on the $^{62}Ni/^{60}Ni$ ratio, the ^{62}Ni signal was kept above 0.5 V. Instrument background

214 signal (typically <10 mV ^{63}Cu) was measured at the beginning of each analytical session.

215 The total procedural blank contained ~1 ng Cu, which equates to <1 % of the Cu sample

216 analyte. Isotope ratios were measured in static mode, with each measurement consisting

217 of 30 cycles of 4.194 second integrations, with a 1 second idle time. Ratios were

218   calculated in the Thermo Neptune Data Evaluation software, which discarded any outliers

219   at the 2-sigma confidence level. To correct for instrumental mass bias, isotope

220   measurements were calculated using the standard sample bracketing protocol relative to

221   the NIST SRM976 standard and corrected for by using the $^{62}Ni/^{60}Ni$ ratio using the

222   exponential law.   Variations in Cu ratios are defined using the delta notation $\delta^{65}Cu$ as

223   follows: $\delta^{65}Cu = [(^{65}Cu/^{63}Cu_{sample}/^{65}Cu/^{63}Cu_{SRM976}) - 1] \times 1000$. Analysis of two separate

224   digestions of USGS standard reference material BHVO-2 gave $\delta^{65}Cu$ of $0.07 \pm 0.06‰$

225   (2SE), in good agreement with literature data (Savage et al., 2015; Moynier et al. 2017).

226

227   Iron isotope measurements follow the protocol of Sossi et al. (2015). Solutions

228   were diluted to 2 ppm, doped with 5 ppm of Ni, and aspirated through a 100μL/min glass

229   nebulizer into a Scott Double Pass-Cyclonic spray chamber coupled to the

230   *ThermoScientific* Neptune Plus MC-ICP-MS. Forty integrations of 4.194 s were

231   performed on the iron shoulder of the peak with medium resolution slits, affording a

232   resolving power, $m/\Delta m$, of 8000; a necessity given the polyatomic ArN, ArO and ArOH

233   interferences that otherwise over-lap with ^{54}Fe, ^{56}Fe and ^{57}Fe respectively. This set-up

234   gave signal intensities of 0.8V for ^{57}Fe and 1V for ^{61}Ni, where Ni corrects for mass bias

235   using the exponential law. The procedural blank for Fe was ≈ 10 ng and resulted in

236   negligible blanks for most of the samples analyzed. Samples were bracketed against the

237   IRMM-014 standard, yielding the delta value: $\delta^{x}Fe$ (‰) = $([^{x}Fe/^{54}Fe]_{sample}/[^{x}Fe/^{54}Fe]_{IRMM-}$

238    $_{014} - 1) \times 1000$, where x is equal to ^{56}Fe or ^{57}Fe. All uncertainties reported on the isotope

239   analyses are the standard deviation of replicates. The total procedural external uncertainty

240   is ± 0.02 (SE) $\delta^{56}Fe$ based on processing and analysis of standard rock powders. Data for

241   standard ETH Hematite, $\delta^{56}Fe = +0.51 \pm 0.02‰$, $\delta^{57}Fe = +0.75 \pm 0.02‰$, agrees with

242   compiled values (Poitrasson et al. 2013).

243

244   **4. Results**

245   Copper and Fe isotope and abundance results are presented in **Tables 1** and **2** and

246   Cu data is shown in **Figure 1**. Bulk samples of 66095 have concentrations of Cu of 4.7

247   and 6.3 μg g^{-1}, in good agreement with ICP-MS data (3.6-5.4 μg g^{-1}), with $\delta^{65}Cu$ of 0.70

248   and 0.79‰. Residue samples generally have a lower range of Cu abundances (2-4.3 μg g^{-}

249    $^{-1}$; except residue J14 at 18.5 µg g^{-1}) and δ^{65}Cu of between 0.59 and 0.77‰. Leaches and

250   etches of HCl and HF-HNO$_3$ have a range in Cu abundances (2.5-11.6 µg g^{-1}) and a wide

251   range in δ^{65}Cu of between 0.63 and 1.38‰. None of the water leaches analyzed for Fe

252   and Zn were analyzed for Cu isotopes due to low total Cu contents.

253

254   Iron isotope and abundance results are presented in **Figures 2** and **3**. All data are

255   mass-dependent in δ^{56}Fe-δ^{57}Fe space conforming to δ^{57}Fe (and its uncertainty) ≈1.5 ×

256   δ^{56}Fe. Iron abundance results obtained on purified Fe fractions for MC-ICP-MS agree

257   well with ICP-MS solution data (**Table 1**), except for a single 1M HCl leach for 66095,

258   430. Bulk samples of 66095 have between 2.2 and 4.8 wt.% FeO and a range of δ^{56}Fe

259   between 0.14 to 0.26‰. Residue samples have lower FeO contents (1.6-2.6 wt.%) and a

260   more restricted range of δ^{56}Fe (0.10 to 0.15‰). Leaches and etches of HCl and HF/HNO$_3$

261   give the widest range of FeO contents (2.3-24.6 wt.%) and heavier δ^{56}Fe (0.15 to 0.19‰)

262   than associated residues. Water leaches have a range in FeO contents (4.0-8.6 wt.%) and

263   the lightest δ^{56}Fe for the dataset (-0.05 to 0.04‰).

264

265   Copper and iron isotopes in 66095 show a much larger relative range in isotopic

266   compositions than for Zn in the same samples. Zinc abundances vary dramatically in

267   whole-rocks, leaches/etches and residues (14.8 to >10,000 µg g^{-1}), but Zn isotopic

268   compositions are generally consistent (-13.5 ±0.3‰, 1SD, n = 12), except for in the water

269   leaches (-13.3 to -8.1‰). None of the measured isotope systems (Fe, Cu, Zn) are

270   correlated with each other for the data set as a whole, or for the bulk, residue or leachate

271   fractionations. Mass balance reconstruction of leachate/etchate and residue experiments

272   versus bulk rock samples of 66095 generally agree well (**Table 2**), with any disagreement

273   likely relating from modal effects between samples, where sample sizes were non-

274   representative of the bulk composition of 66095.

275

276   **4.   Discussion**

277   ***4.1   Copper and iron isotope composition of 66095 and the Moon***

278   Prior to discussing the distribution of moderately volatile elements in the Rusty

279   Rock, 66095, it is useful to place the Cu and Fe isotope compositions in context with

280   lunar compositions. In the first instance, while there is a meteoritic component in the

281   Rusty Rock, the amount of impact contamination is not enough to explain either the Cu

282   or Fe contents of 66095 (Day et al., 2017). Instead, the Moon provides a key comparison

283   with the composition of the Earth, with prior work indicating strong geochemical

284   similarities between the two bodies (Ringwood & Kesson, 1977; O'Neill, 1991). For

285   example, Li, O, Si, Mg, Ca, Ti, Fe, and Sr stable isotopic compositions for the Earth and

286   Moon are all identical within analytical uncertainties (e.g., Spicuzza et al., 2007; Liu et

287   al., 2010; Moynier et al. 2010; Sedaghatpour et al., 2013; Valdes et al., 2014; Day et al.,

288   2016; Millet et al., 2016; Young et al., 2016; Sossi & Moynier, 2017). For moderately

289   volatile elements such as S, Cl, K and Zn, however, the Moon is highly distinctive

290   compared with Earth (e.g., Day & Moynier, 2014, Wang and Jacobsen 2016). To date,

291   there are limited Cu isotopic data available for lunar rocks and therefore the composition

292   of the bulk silicate Moon (BSM) is not well-constrained, while the BSM δ^{56}Fe

293   composition has been estimated from lunar Mg-suite rocks at +0.05 ± 0.02‰ (Sossi &

294   Moynier, 2017); indistinguishable to slightly heavier than bulk silicate Earth (BSE)

295   values of +0.03 ±0.03‰ (Craddock et al., 2013) and +0.05 ± 0.01‰ (Sossi et al., 2016).

296   The estimated BSM δ^{56}Fe value from the Mg-suite samples is ~0.07‰ lighter than the

297   low-Ti mare basalt average of +0.12 ± 0.02‰ (Liu et al. 2010; **Figure 3**), reflecting iron

298   isotopic fractionation of melts from the lunar interior during magmatic differentiation

299   processes (see discussion in Sossi and Moynier, 2017).

300

301   As a comparison for the Cu isotopic composition, we compiled data from the

302   literature for a range of lunar rock types, including regolith or soil samples, mare basalts

303   and pyroclastic glass beads that collectively span a wide-range of δ^{65}Cu values (-1 to

304   +4.5‰) and Cu concentrations (2.7 to 84 µg g^{-1}; **Figure 1**). Lunar soil samples are

305   consistently isotopically heavy for both δ^{65}Cu (+0.3 to +4.5‰) and δ^{66}Zn (+2.2 to

306   +6.4‰), with generally low Cu abundances (3 to 84 µg g^{-1}); these characteristics of lunar

307   soils have previously been attributed to impact gardening and sputtering effects (Herzog

308   et al., 2009). The pyroclastic glass beads (74001, 74220) have typically higher Cu

309   abundances (average = ~20 µg g^{-1}) and isotopically lighter δ^{65}Cu (0.15 to –1‰) and

310   δ^{66}Zn compositions than most basalts, which reflect addition of isotopically light Cu- and

311   Zn-rich condensate material to these deposits (Moynier et al., 2006; Herzog et al., 2009;

312   Kato et al., 2015; Day et al., 2017). Mare basalts span a range of Cu abundances (~2.7 to

313   26 $\mu g\ g^{-1}$) exceeding abundances for the most primitive mare basalts (Day, 2018), and

314   have $\delta^{65}Cu$ values between -0.1 and 2.0‰.

315

316   It has previously been assumed that mare basalts are proxies for lunar mantle Zn

317   isotope compositions (e.g., Paniello et al., 2012). Making a similar assumption for Cu,

318   pristine mare basalts should have low Cu. This is because Cu content is predicted to be

319   low in the lunar mantle, and hosted within sulfide phases (O'Neill, 1991). Sulfide

320   exhaustion in the lunar mantle occurs after around 8% partial melting due to low S

321   contents, leading to the prediction that low Cu contents occur in primary lunar mantle

322   melts (<10 $\mu g\ g^{-1}$; Day, 2018). Mare basalts with low Cu contents have $\delta^{65}Cu$ = +0.92

323   ±0.16‰. This composition is significantly isotopically heavier than typical terrestrial

324   igneous rock compositions (–0.07 to +0.16‰), or the BSE estimate (+0.07 ±0.10‰; 2

325   S.D.; Savage et al., 2015). The heavier estimated $\delta^{65}Cu$ of lunar mare basalt sources

326   relative to the BSE is similar to the differences observed for Rb, Cl, K, Zn and S isotopes

327   in the Moon, and consistent with high-temperature processing implied by the depletion in

328   moderately volatile elements in the lunar interior compared with the terrestrial mantle

329   (Day & Moynier, 2014; Wang & Jacobsen, 2016; Pringle & Moynier, 2017).

330

331   It has previously been shown that 66095 is depleted in the heavier isotopes of Zn,

332   distinguishing it from mare basalt compositions (Day et al., 2017). It is therefore

333   remarkable that bulk sample, residue and acid reagent treatments (HCl, HF-HNO$_3$) of

334   66095 are broadly within the range of lunar mare basalt values for $\delta^{65}Cu$ and $\delta^{56}Fe$ (or

335   $\delta^{57}Fe$) and Cu concentrations. The only materials from 66095 that show values

336   significantly outside of these ranges are the isotopically heavy bulk breccia sample

337   (66095, 430), and the isotopically light water leach treatments for iron isotopes. For the

338   water leaches, it is likely that they accessed soluble and isotopically light FeCl salts, or

339   akaganéite.

340

341   The heavy Fe isotopic value in 66095, 430 relates to the highest Fe content of the

342   dataset and is consistent with sampling of impact-generated Fe-metal grains formed by

343   partial impact-vaporization and preferential loss of light Fe isotopes, as proposed

344   previously by Wang et al. (2012). Prior work on terrestrial analog systems have

345   demonstrated that large (2-3‰) Fe isotope fractionations occur due to redox reactions

346   between ferrous and ferric species (e.g., Hill & Schauble, 2008; Polyakov & Soultanov,

347   2011; Syverson et al., 2017). However, in the case of the Moon, where the majority of Fe

348   speciation is considered to be ferrous (Fe^{2+}) or native (Fe^0), such fractionations are likely

349   to be of lower relevance. Theoretical studies indicate that changes in bond partners (i.e.,

350   different ligands or coordination numbers) should result in significant isotopic

351   fractionation, but conditions similar to those attained on airless bodies have not been

352   well-constrained. Empirical stidy of nanophase iron ($_{np}Fe^0$) show large enrichments in the

353   heaviest Fe isotopes ($\delta^{56}Fe$ up to 0.71%) compared with lunar mare basalts (Wang et al.,

354   2012). These results indicate that impact vaporization processes can lead to enrichment of

355   heavy Fe isotopes in the residues and light Fe isotopes in the vapor, consistent with the

356   Fe isotopic variations in components of 66095 and its origin as an impact melt breccia.

357   Further experiments would be valuable to elucidate this effect.

358

359   Mass-balance calculations for leaching and residue experiments yield similar

360   values to bulk samples of 66095 (**Table 2**), with 3.0 ±1.3 wt.% FeO (range = 2.0-4.8

361   wt.%), 5.4 ±3.1 ppm Cu (range = 3-12 ppm), with average $\delta^{56}Fe$ of 0.15 ± 0.05‰

362   (weighted mean = 0.16‰) and $\delta^{65}Cu$ of 0.72 ±0.14‰ (weighted mean = 0.78‰). The

363   new results for Cu and Fe isotope compositions of 66095 show that they are not

364   particularly anomalous relative to baseline lunar compositions defined by mare basalts

365   ($\delta^{65}Cu$ = +0.92 ± 0.16‰; $\delta^{56}Fe$ = +0.12 ± 0.02‰). In the following sections, we outline

366   the importance of these observations for volatile element behavior in and on the Moon.

367

4.2   *Origin of volatile element enrichments in the Rusty Rock, 66095*

369   The fine-grained subophitic to ophitic polymict breccia 66095, is the archetypal

370   lunar 'Rusty Rock', recognized as an important sample during initial characterization

371   with the discovery of rust coloured stains on its surface and interior (Bass, 1972; Taylor

372   et al., 1973; El Goresy et al., 1973). The 'rusty' character of 66095 is due to the presence

373   of akaganéite (FeOOH; Taylor et al., 1973) and lawrencite (FeCl$_2$; Shearer et al., 2014).

374   Subsequently, greater than twenty-five Apollo 16 samples have been identified as having

375   rusty rims of iron hydroxide phases around FeNi metal, as FeO(OH) polymorphs

376   (akaganéite, βFeO[OH,Cl]) (Colson, 1992; Jean et al., 2016). These samples come from

377   nearly all sampled stations of the Apollo 16 mission to the Cayley Plains and include rake

378   samples in soils (68501, 68441), regolith breccias (60016, 61135, 65095, 66035, 66036),

379   polymict or dark matrix breccias (60255, 66055, 69935), impact melt rocks and breccias

380   (60625, 63585, 64455, 64567, 66095), and anorthosite and anorthositic breccias (65326,

381   67016, 67455). The presence of rusty alteration both within different rock types from the

382   Apollo 16 site, and from different locations across the site suggests a common process

383   responsible for the alteration.

384

385   In addition to the pervasive low temperature, volatile-rich oxyhydrated mineral

386   assemblages, 66095 is also enriched in a volatile component, including elevated

387   abundances of Bi, Br, Cd, Cl, Ge, I, ^{204}Pb, Sb, Tl and Zn compared with other lunar

388   samples (Krahenbuhl et al., 1973; Wanke et al., 1981; Jovanovic & Reed, 1981; Ebihara

389   et al., 1992; Day et al., 2017). Amongst these elements, the chlorine composition of

390   66095 is isotopically heavier (δ^{37}Cl = +14.0 to +15.6‰) than any known terrestrial rock

391   samples (typically -3 to +3‰), and consistent with δ^{37}Cl values (+5.6 to +15.7‰) for

392   lunar rocks and soils around the Apollo 16 site (Shearer et al., 2014). The Rusty Rock

393   also has one of the most extreme, isotopically light Zn compositions measured for any

394   Solar System material (δ^{66}Zn = -13.5‰; Day et al., 2017), again inconsistent with a

395   terrestrial origin, where δ^{66}Zn is typically between 0.1 and 0.4‰ in terrestrial rocks

396   (Paniello et al., 2012; Moynier et al., 2017).

397

398   Amongst the volatile elements, the U-Pb and Rb-Sr isotope systems are tracers

399   *par excellence* of volatile enrichment and depletion since they can both potentially

400   provide chronological information, and, in the case of the U-Pb isotope system, the parent

401   (U) is refractory, and the daughter (Pb) is volatile, whereas the opposite is true for the

402   Rb-Sr isotope system. The lead isotopic composition of 66095 shows that greater than

403   85% of Pb is unsupported in the rock, identifying a source with high-μ ($^{238}U/^{204}Pb \geq 570$;

404   Nunes & Tatsumoto, 1973). The age defined from ^{207}Pb-^{206}Pb chronology (4.01 ±0.06

405   Ga) is identical within uncertainty of the ^{87}Rb-^{87}Sr age (4.06 ±0.24 Ga), with the defined

406    $^{87}Sr/^{86}Sr$ initial of 0.69909 ±5, consistent with lunar origins for both isotope systems (Day

407   et al., 2017).

408

409   Strontium and Pb isotope compositions suggest a long-term volatile-depleted

410   source for 66095, in apparent contradiction to the enrichment in volatile components in

411   the sample (e.g., Bi, Br, Cd, Cl, Ge, I, ^{204}Pb, Sb, Tl, Zn). These geochemical

412   characteristics can be reconciled by outgassing of an already volatile-depleted source

413   within the Moon to generate the volatile enriched character of 66095 (Day et al., 2017).

414   Such a model is consistent with fumarolic activity (e.g., Krahenbuhl et al., 1973; Nunes

415   & Tatsumoto, 1973), where lawrencite was deposited at between 650°C to 570°C

416   (Shearer et al., 2014) and sphalerite was deposited at between 200°C and 600°C (Day et

417   al., 2017) from an H-poor gas phase. Shearer et al. (2014) further proposed that the low H

418   gas phase was metal chloride bearing, depositing Zn, Cu, Pb and Fe. In detail, however,

419   the cause of Zn and Pb volatile enrichment must be distinct from Cu and Fe in 66095,

420   based on stable isotope composition. The 'rusty' character and volatile element

421   enrichment of 66095 is therefore consistent with volatile enrichment through fumarolic

422   activity – likely during impact processes - from a volatile-poor source in the Moon, as

423   opposed to partly to fully representing terrestrial alteration products, as had been

424   suggested previously (Epstein & Taylor, 1974; Taylor et al., 1974).

425

4.3   *Causes of Fe, Cu, Pb and Zn isotopic and abundance variability in 66095*

427   A notable feature of the new Cu and Fe isotope data for 66095 is that the values

428   for bulk samples, residues after leaching and HF/HNO$_3$ treatment samples generally all

429   lie within or close to the range of mare basalts (**Figures 1** and **3**).

430

431   To compare the relative enrichments of elements in 66095, data for Cl from

432   Shearer et al. (2014), Sb, Se, Te, Ag, Br, Bi, Cd and Tl from Krahenbuhl et al. (1973) and

433   data for all other elements from Day et al. (2017), are compared with the average lunar

434   volatile depletion trend (**Figure 4**). A notable aspect of this plot is that two distinct

435   groups of moderately volatile elements (here defined as elements with $T_c 50\% < Fe$) can

436   be distinguished; those that are equally or more depleted than the average lunar volatile

437   depletion trend (Bi, Se, Te, Ge, Cu, Ag, Sb, Mn, P, Cr) and those that are significantly

438   more enriched compared to this trend (Tl, Br, Cd, Sn, Zn, Pb, Rb, Cs, Ga, B, Cl, Li).

439   Concentrations of moderately volatile elements (e.g., Cr, Mn, Cu, Rb, Cs, Zn) measured

440   on different aliquots of 66095 can vary significantly (e.g., Krahenbuhl et al., 1973;

441   Wanke et al., 1981; Ebihara et al., 1992, and see Table S2 of Day et al., 2017), but the

442   same general trends are observed no matter which data are used, suggesting that the

443   observation of two groups of depleted and enriched moderately volatile elements (MVE)

444   is robust.

445

446   Instead of the original description of 66095 being enriched in Bi, Br, Cd, Cl, Ge,

447   I, [204]Pb, Sb, Tl, Zn, we redefine the moderately volatile enrichment as occurring for Tl,

448   Br, Cd, Sn, Zn, Pb, Rb, Cs, Ga, B, Cl, Li (enriched MVE) and that Bi, Se, Te, Ge, Cu,

449   Ag, Sb, Mn, P and Cr are all relatively depleted (depleted MVE), compared with the

450   average lunar depletion trend. There are two likely reasons for the differences in the

451   relative enrichment of depletion of these MVE with 66095. First, some of the depleted

452   MVE group are inherent to the sample, being dominantly located within minerals and

453   phases associated with the breccia and clasts making up 66095, rather than as

454   condensates. This can be demonstrated for Fe, where the dominant Fe-rich phase in the

455   Rusty Rock are olivine (~10 modal %; Fo_{77}), pyroxene (~30 modal %; $Wo_7En_{72}Fs_{20}$ to

456   $Wo_{17}En_{65}Fs_{18}$), and FeNi metal (~1.2 modal %; Lunar Compendium). Components that

457   make up 66095 are generally low in FeO (1.4-9.6 wt.%; Wanke et al., 1981; this study)

458   and the mass balance for Fe can therefore be fully accounted for by these phases. Metal

459   phases are the dominant source of Cu, where Cu solubility in sphalerite is low (Scott,

460   1983), and FeNi metal in some Apollo 16 impact melt rocks have up to 0.5 wt.% Cu

461   (McIntosh et al., 2018). Even assuming the average Cu content of FeNi metal grains in

462   impact melt rocks of ~0.1 wt.% Cu, 1.2 modal% FeNi metal in 66095 would give ~12

463   ppm Cu in bulk samples of 66095, which is well within the range of Cu contents

464   measured for the 'Rusty Rock' (**Table 1**).

465

466   The second reason for different distributions of moderately volatile elements in

467   66095 is due to the role of condensate and vapor deposition, where the enriched MVE

468   group are presumed to have been primarily enriched by such a process. As noted

469   previously, sphalerite and lawrencite were deposited between 200 and 650°C, which

470   would be consistent, for example, with deposition of discrete grains of (Zn,Fe)S or PbS

471   (?) and $(Fe,Ni)Cl_2$. While some elements appear to be dominantly controlled by primary

472   phases, leaching and etching experiments have the potential to reveal possible condensate

473   or vapour additions, one example being the water leaches measured for Fe isotope

474   compositions (**Table 1**). These water leaches are all isotopically light with respect to Fe

475   ($\delta^{56}Fe$ = 0.04 to -0.05‰) and have low total abundances of Fe (0.7 to 20 µg g^{-1}). The low

476    $\delta^{56}Fe$ do not reflect analytical blanks, which represent less than 1.4% of the total

477   measured Fe in the samples. The water leach iron isotope compositions are also mass-

478   dependent. Although an extremely minor component of 66095, there appears to be

479   isotopically light Fe within or on 66095, and this may originate from FeCl salts, either

480   directly, or from the breakdown of lawrencite in H_2O, where water leaches have high

481   concentrations of both Fe and Ni (c.f., Table S2 of Day et al., 2017). Examples of

482   location of elements within 66095 and how they were inherited in the sample are given in

483   **Figure 5**, where primary grains of FeNi metal – hosts to both Fe and Cu - are distinct

484   from the secondary sphalerite and veins and infilled fractures of Cl-rich materials.

485

486   The composition of moderately volatile elements in the 'Rusty Rock' would

487   imply that it formed at lower temperatures away from a fumarolic vent, consistent with

488   lawrencite and sphalerite thermometry (Shearer et al., 2014; Day et al., 2017). The

489   distribution of moderately volatile trace elements in the 'Rusty Rock', 66095, appear to

490   follow the expected trend of element deposition from a lunar volcanic gas. Renggli et al.

491   (2017) calculated the speciation of Ni, Fe, Cu, Ga, Zn and Pb for a lunar volcanic gas

492   composition at 2 log units below the Iron-Wüstite buffer over a range of temperatures

493   (500 to 1500°C and pressures (10^{-6} to 1 bar). For a lunar composition gas, the major

494   volatiles were likely to be CO, H_2, H_2S, COS and S_2. These authors concluded that

495   deposition with decreasing temperature and increasing pressure occurs in the order: Ni ≈

496   Fe > Cu > Ga > Zn > Pb. In general, at 10^{-6} bar, these metals exist as monatomic gases at

497   higher temperatures, whereas the gaseous chloride species of Cu and Fe become

498   predominant below 800 °C. As such, native metals tend to precipitate close to the

499   volcanic or fumarolic vent at higher temperatures, with sulfide or chloride species

500   distributed further away. The composition of moderately volatile elements in the 'Rusty

501   Rock' would imply that it formed at lower temperatures away from a fumarolic vent,

502   consistent with the lawrencite and sphalerite thermometry (**Figure 4**). Iron is present as

503   chlorides and oxy-hydroxides that are only stable at low temperatures (<700 °C),

504   implying the persistence of iron in the vapour below 1200-1300 °C as modelled by

505   Renggli et al. (2017). The fact that the Cu and Fe isotope composition of the Rusty Rock

506   is within the range of mare basalts leaves two options. First, that Cu and Fe were not

507   transported in the gas and are instead dominated by inherent mineralogical components,

508   and second that the Cu and Fe budget of the rock condensed entirely and was thus

509   associated with negligible isotope fractionation with respect to its source.

510

511   The first option is consistent with the observation that Cu and Fe are not enriched

512   with respect to mare basalts (**Figure 4**). However, that Fe-rich and isotopically light

513   deposits occur on the surface from water leaches attests to some transport of Fe (and the

514   more volatile Cu) in the vapor phase. As discussed above, the quantity that these surface

515   deposits comprise of the total Cu and Fe budget of the rock is minor, and the leachates

516   are not significantly fractionated relative to the bulk rock dissolution. This implies that,

517   although Cu and Fe were transported in the vapor, they were not sufficiently enriched to

518   modify the composition of the bulk rock. Moreover, that the leachates have compositions

519   overlapping with mare basalts argues that the budget of Cu and Fe in the vapor suggests

520   that they condensed fully from the vapor phase such that their isotopic composition

521   should reflect that of their sources (option 2). Therefore, the lunar source from which the

522   vapour was derived was similar in nature to that of mare basalts. Therefore, a distinct,

523   isotopically-fractionated, volatile-enriched reservoir in the lunar mantle in unlikely.

524

525   The isotopically 'normal' nature of Cu and Fe in sample 66095 is seemingly at-

526   odds with the strongly fractionated Zn isotope composition (-13.6±0.3 ‰) in the same

527   sample. A possible explanation for the distinct behavior of Zn relates to its volatility; Zn

528   (and Pb) is calculated to precipitate from a gas of lunar composition at lower

529   temperatures than are Cu and Fe (Renggli et al. 2017). Therefore, the strongly negative

530   δ^{66}Zn implies condensation of the gas at temperatures at which Zn is only partially

531   condensed, resulting in isotopically light condensates. This temperature must have been

532   sufficiently low to have permitted complete condensation of Cu and Fe and to have

533   stabilized Fe-chlorides. Together, these constraints imply precipitation of the gas phase

534   below 900 °C but above 700 °C (at total pressures of 10^{-6} bar and IW-2). That Cu and Fe

535   elements are not enriched in the sample supports lower abundance in the gas phase

536   relative to the source rock. By contrast, that Zn (and Pb) are enriched points to their

537   higher relative abundance in the gas phase compared to the sample, even if Zn has only

538   undergone partial condensation. This scenario would predict strong mass-dependent

539   isotopic fractionation in elements more volatile than Zn, such as Pb, and others that are

540   enriched in sample 66095 (Tl, Cd; **Figure 4**). Gallium isotopes may be particularly

541   exacting because Ga is predicted to condense at temperatures between those of Cu and

542   Zn.

543

544   *4.4   Implications for volatile reservoirs at the surface and in the lunar interior*

545   The Rusty Rock, 66095, is one of the most volatile-rich rocks recovered from the

546   Moon, having experienced modification by fumarolic activity resulting in the enrichment

547   in some volatile and moderately volatile elements (Krahenbuhl et al., 1973; Nunes &

548   Tatsumoto, 1973). The source of these volatiles, however, is quite volatile-poor, being

549   particularly evident from combined Zn, Cl, Pb and ^{87}Sr/^{86}Sr isotope data indicating

550   addition of condensate material with isotopically heavy Cl, isotopically light Zn, low

551   long-term Rb/Sr and unsupported Pb (Day et al., 2017). The high Zn content and

552   extremely isotopically light δ^{66}Zn are particularly notable features of 66095, making the

553   sample distinct from all other lunar rocks. Here we have shown that for Fe and Cu

554   isotopes, 66095 is not particularly anomalous compared with mare basalts, with these

555   isotope systems being controlled by Fe and Cu within FeNi metal and/or silicate phases

556   within the sample, rather than from phases introduced by fumarolic activity (e.g.,

557   sphalerite, Cl in veins). These observations have two important implications, the first

558   relating to volatile-rich pyroclastic glass beads, and the second to the distribution of

559   volatile elements on the lunar surface.

560

561   The pyroclastic glass beads (15426, 74220) are volatile-rich samples from the

562   Moon that were formed by fire fountaining and have high Cu (7 to 32 ppm) and Zn (50 to

563   230 ppm) concentrations and isotopically light Cu (δ^{65}Cu = +0.1 to -1‰) and Zn (δ^{66}Zn =

564   −1‰ to −4‰) that correlate with bead size (Herzog et al., 2009; Kato et al., 2015). The

565   Zn and Cu isotope compositions in these samples reflect condensates on the surfaces of

566   the beads, as there are no phases dominantly controlling Cu or Zn in the samples, and

567   with direct observation of Zn-bearing minerals on the outsides of the beads (Ma & Liu,

568   2019). The volcanic glasses have been shown to have significant enrichments in volatile

569   elements that are surface correlated (Krahenbuhl, 1980), with lower estimated μ

570   (^{238}U/^{204}Pb = 19 to 55) than mare basalts (300 to 600; Tatsumoto et al., 1987), and high

571   δ^{37}Cl in leachates from 74220 (+8.6 to +9.6‰; Sharp et al., 2010). The volcanic glasses

572   also have chondritic relative abundances of the HSE on their outer edges (Walker et al.,

573   2004), with absolute abundances of these elements that are greater than in mare basalts

574   (Day et al., 2007; Day & Walker, 2015). Collectively, these lines of evidence suggest that

575   the volcanic glass beads have lunar condensate, as well as impactor materials, on their

576   surfaces, both for Zn, as well as for Cu. The information on volatile contents in the Rusty

577   Rock 66095 indicates that such material was likely added during fire fountaining, or after

578   the formation of the glass bead deposits. The new results for Cu in 66095 would therefore

579   suggest that the lunar pyroclastic glass beads are anomalously enriched in a condensate

580   volatile component from a dominantly 'dry' lunar interior.

581

582   A volatile-rich lunar surface has been inferred from remote sensing mission data,

583   including Clementine, Lunar Prospector, Lunar Reconnaissance Orbiter (LRO), the Moon

584   Mineralogy Mapper (M^3) on Chandrayaan-1, and the Lunar Crater Observation and

585   Sensing Satellite (LCROSS). Data from these missions have been used to identify H-

586   bearing species not only within permanently-shadowed cold traps at polar regions, but

587   also in non-polar regions of the Moon (e.g. Feldman et al., 1998; Pieters et al., 2009;

588   Paige et al., 2010; Colaprete et al., 2010; Li & Milliken, 2017). Most of this volatile

589   component has been attributed to solar wind implantation during agglutinate formation

590   (Li & Milliken, 2017). The 'Rusty Rock' 66095 offers the possibility that a significant

591   fraction of volatiles trapped within some lunar regolith may originate from interior

592   sources and is isotopically strongly fractionated due to the volatile depleted nature of the

593   lunar interior. The fumarolic activity required to form the volatile enriched 'Rusty Rocks'

594   at the Cayley Plains may not be a localized feature, or a temporally limited event, with

595   recent disturbance structures attributed to outgassing occurring at Ina Crater (e.g. Schultz

596   et al., 2006). Testing what fraction of lunar volatile deposits originate from the interior of

597   the Moon should be possible using isotopic fingerprinting of solar wind implantation

598   versus kinetic isotopic fractionation during vapour-phase and condensate reactions.

599

600   **5.   Conclusions**

601   Copper and iron isotope and abundance compositions measured in bulk-rocks,

602   residues and acid leaches span a relatively limited range of compositions (3.0 ±1.3 wt.%

603   FeO [range = 2.0-4.8 wt.%], 5.4 ±3.1 ppm Cu [range = 3-12 ppm], average $\delta^{56}Fe$ of 0.15

604   ± 0.05‰ (weighted mean = 0.156‰) and $\delta^{65}Cu$ of 0.72 ±0.14‰ (weighted mean =

605   0.78‰). The stable isotope compositions of Cu and Fe are similar to averages of mare

606   basalts ($\delta^{65}Cu$ = +0.92 ±0.16‰; $\delta^{56}Fe$ = +0.12 ± 0.02‰) and are therefore less extreme

607   compositional variations than previously measured for $\delta^{66}Zn$ (-13.5 ±0.3‰), $\delta^{37}Cl$ (+14

608   to +15.6‰). Combined with the high $^{206}Pb/^{204}Pb$ and low $^{87}Sr/^{86}Sr$ measured in 66095,

609   these results are consistent with the enrichment in volatile elements in the 'Rusty Rock'

610   by fumarolic activity and preferential enrichment of volatiles elements from a cooling gas

611   originating from a volatile-poor lunar interior. We find that the enrichment in Tl, Br, Cd,

612   Sn, Zn, Pb, Rb, Cs, Ga, B, Cl, Li relative to Bi, Se, Te, Ge, Cu, Ag, Sb, Mn, P, Cr and Fe

613   is consistent with volcanic outgassing models, and indicates that 66095 may have formed

614   distal from the original source of the gas. The evidence for impact brecciation and the

615   moderately elevated HSE contents of 66095 are consistent with fumarolic activity in the

616   vicinity of the Apollo 16 site at the Cayley Plains, induced by impact heating. The

617   elucidation of the volatile-rich character of 66095 explains the 'rusting' and alteration on

618   the sample, through fumarolic activity, alteration and deposition of volatile and

619   moderately volatile elements, as well as demonstrating that volatile-rich rocks can occur

620   on the lunar surface from outgassing of the volatile-poor lunar interior. Our results for Cu

621   and Zn isotopes demonstrate that the phases hosting these elements can play an important

622   role in dictating isotopic composition, leading to apparently 'mixed messages' regarding

623   the source of volatiles in lunar samples.

624

636

637   **REFERENCES**

638   Albarède, F., Albalat, E., Lee, C.T.A. (2015) An intrinsic volatility scale relevant to the
639   Earth and Moon and the status of water in the Moon. Meteoritics & Planetary Science
640   50, 568-577.
641   Bass, M.N. 1972. Description of 66095. In: Apollo 16 Lunar Sample Information
642   Catalog, 268-274. MSC-03210, NASA Johnson Space Center, Houston.
643   Bonnand, P., Parkinson, I.J., Anand, M., 2016. Mass dependent fractionation of stable
644   chromium isotopes in mare basalts: implications for the formation and the
645   differentiation of the Moon. Geochimica et Cosmochimica Acta, 175, 208-221.
646   Boyce, J.W., Treiman, A.H., Guan, Y., Ma, C., Eiler, J.M., Gross, J., Greenwood, J.P.,
647   Stolper, E.M., 2015. The chlorine isotope fingerprint of the lunar magma ocean.
648   Science advances, 1, e1500380.
649   Chen, Y., Zhang, Y., Liu, Y., Guan, Y., Eiler, J., Stolper, E.M., 2015. Water, fluorine,
650   and sulfur concentrations in the lunar mantle. Earth and Planetary Science Letters 427,
651   37-46.
652   Colson, R.O., 1992. Mineralization on the moon? Theoretical considerations of Apollo 16
653   'rusty rocks', sulfide replacement in 67016, and surface-correlated volatiles on lunar
654   volcanic glass. Lunar and Planetary Science Conference Proceedings, 22, 427-436.

655 Colaprete, A., Schultz, P., Heldmann, J., Wooden, D., Shirley, M., Ennico, K., Hermalyn,
656   B., Marshall, W., Ricco, A., Elphic, R.C., Goldstein, D., 2010. Detection of water in
657   the LCROSS ejecta plume. Science, 330, 463-468.
658 Craddock, P.R., Warren, J.M. and Dauphas, N., 2013. Abyssal peridotites reveal the near-
659   chondritic Fe isotopic composition of the Earth. Earth and Planetary Science Letters,
660   365, 63-76.
661 Day, J.M.D. 2018. Geochemical constraints on residual metal and sulfide in the sources
662   of lunar mare basalts. American Mineralogist, 103, 1734-1740.
663 Day, J.M.D., Moynier, F. 2014. Evaporative fractionation of volatile stable isotopes and
664   their bearing on the origin of the Moon. Phil. Trans. R. Soc. London Ser. A 372, 2024,
665   20130259.
666 Day, J.M.D., Walker, R.J. 2015. Highly siderophile element depletion in the Moon. Earth
667   and Planetary Science Letters, 423, 114-124.
668 Day J.M.D., Pearson D.G., Taylor L.A., 2007. Highly siderophile element constraints on
669   accretion and differentiation of the Earth-Moon system. Science, 315, 217-219.
670 Day, J.M.D., Qin, L., Ash, R.D., McDonough, W.F., Teng, F.-Z., Rudnick, R.L., Taylor,
671   L.A. 2016. Evidence for high-temperature fractionation of lithium isotopes during
672   differentiation of the Moon. Meteoritics and Planetary Science, 51, 1046-1062.
673 Day, J.M.D., Moynier, F., Shearer, C.K. 2017. Late-stage magmatic outgassing from a
674   volatile-depleted Moon. Proceedings of the National Academy of Sciences, 114, 9457-
675   9551.
676 Dhaliwal, J.K., Day, J.M.D., Moynier, F., 2018. Volatile element loss during planetary
677   magma ocean phases. Icarus, 300, 249-260.
678 Ebihara, M., Wolf, R., Warren, P.H., Anders, E., 1992. Trace elements in 59 mostly
679   highland moon rocks. In Lunar and Planetary Science Conference Proceedings 22,
680   417-426.
681 Epstein, S., Taylor Jr, H.P., 1974. D/H and O-18/O-16 ratios of H_2O in the 'rusty' breccia
682   66095 and the origin of 'lunar water'. Lunar and Planetary Science Conference
683   Proceedings, 5, 1839-1854).
684 Feldman, W.C., Maurice, S., Binder, A.B., Barraclough, B.L., Elphic, R.C., Lawrence,
685   D.J., 1998. Fluxes of fast and epithermal neutrons from Lunar Prospector: Evidence
686   for water ice at the lunar poles. Science, 281, 1496-1500.
687 Garrison, J.R., Taylor, L.A. 1980. Genesis of highland basalt breccias: a view from
688   66095. In: Papike J.J., Merrill, M., Eds. Proceedings of the Conference on the Lunar
689   Highlands Crust, Geochimica et Cosmochimica Supplement, 12, 395-417.
690 Hauri, E.H., Weinreich, T., Saal, A., Rutherford, M., Van Orman, J.A., 2011. High Pre-
691   Eruptive Water Contents Preserved in Lunar Melt Inclusions. Science, 333, 213-215.
692 Herzog, G.F., Moynier, F., Albarède, F., Berezhnoy, A.A., 2009. Isotopic and elemental
693   abundances of copper and zinc in lunar samples, Zagami, Pele's hairs, and a terrestrial
694   basalt. Geochimica et Cosmochimica Acta 73, 5884-5904.
695 Hill, P., Schauble, E.A., 2008. Modeling the effects of bond environment on equilibrium
696   iron isotope fractionation in ferric aquo–chloro complexes. Geochimica et
697   Cosmochimica Acta, 72, 1939–1958.
698 Hunter, R.H., Taylor, L.A. 1981. Rusty rock 66095: a paradigm for volatile-element
699   mobility in highland rocks. Proceedings of the 12th Lunar and Planetary Science
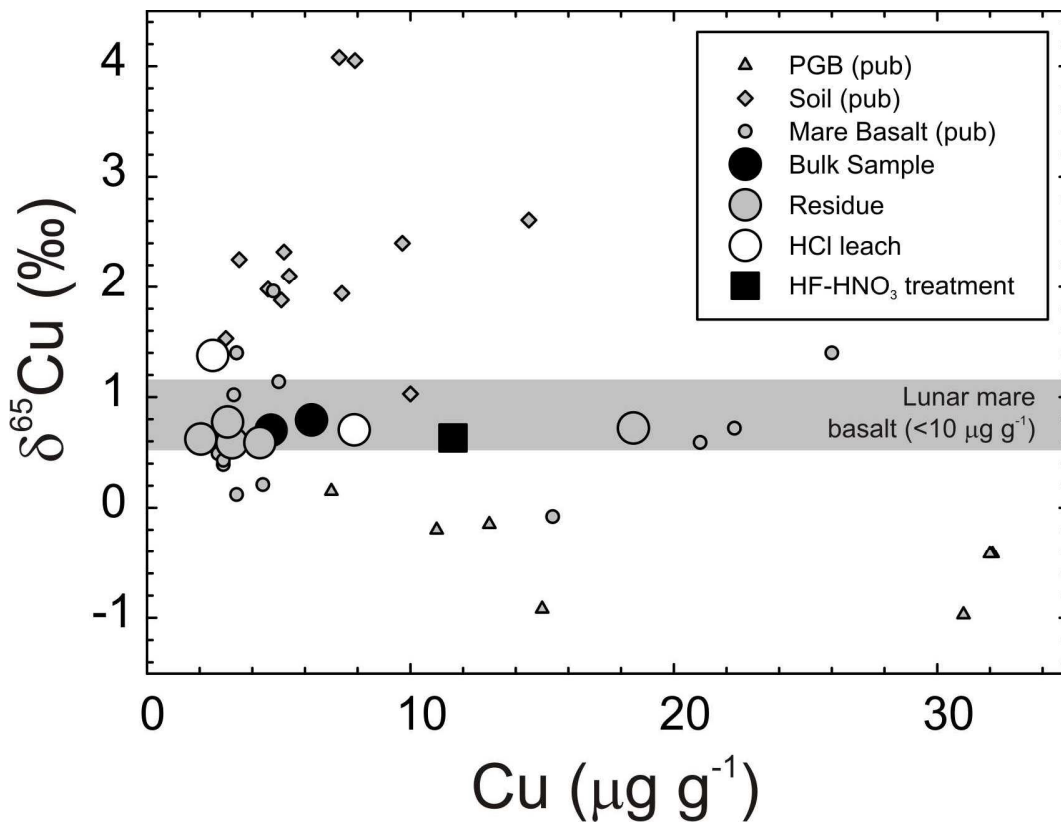700   Conference, 261-280.

701   Jean, M.M., Bodnar, R., Farley, C., Taylor, L.A. 2016. 'Rusty Rocks' from the Moon:
702   Volatile-Element Contributions from Meteorites. Lunar and Planetary Science
703   Conference, 47, 2498.
704   Jones, J.H., Palme, H., 2000. Geochemical constraints on the origin of the Earth and
705   Moon. In: Canup, R.M., Righter, K. (Eds.) Origin of the Earth and Moon, University
706   of Arizona Press, Tucson, 197-216.
707   Jovanovic S., Reed G.W. 1981. Aspects of the history of 66095 based on trace elements
708   in clasts and whole rock. Proc. 12th Lunar Planet. Sci. Conf. 295-304.
709   Kato, C., Moynier, F., Valdes, M.C., Dhaliwal, J.K., Day, J.M.D. 2015. Extensive
710   volatile loss during formation and differentiation of the Moon. Nature
711   Communications, 6.
712   Krahenbuhl, U., Ganapathy, R., Morgan, J.W., Anders, E. 1973. Volatile elements in
713   Apollo 16 samples: Implications for highland volcanism and accretion history of the
714   moon. Proc. 4th Lunar Sci. Conf. 1325-1348.
715   Li, S., Milliken, R.E., 2017. Water on the surface of the Moon as seen by the Moon
716   Mineralogy Mapper: Distribution, abundance, and origins. Science advances, 3,
717   p.e1701471.
718   Liu Y., Spicuzza M.J., Craddock P.D., Day J.M.D., Valley J.W., Dauphas N., Taylor
719   L.A. 2010. Oxygen and iron isotope constraints on near-surface fractionation effects
720   and the composition of lunar mare basalt source regions. Geochimica et
721   Cosmochimica Acta, 74, 6249-6262.
722   Lindsay, F.N., Herzog, G.F., Albarède, F., Korotev, R.L., 2011, Elemental and Isotopic
723   Abundances of Fe, Cu and Zn in Low-Ti Basalts. Lunar and Planetary Science
724   Conference, 42, 1907.
725   Lodders, K., 2003. Solar system abundances and condensation temperatures of the
726   elements. The Astrophysical Journal, 591, 1220.
727   Ma, C., Liu, Y., 2019. Discovery of zinc-rich mineral on the surface of lunar orange
728   pyroclastic beads. American Mineralogist 10.2138/am-2019-6896.
729   Maréchal, C.N., Télouk, P., Albarède, F., 1999. Precise analysis of copper and zinc
730   isotopic compositions by plasma-source mass spectrometry. Chemical Geology, 156,
731   251-273.
732   McDonough, W.F., Sun, S.S., 1995. The composition of the Earth. Chemical Geology,
733   120, pp.223-253.
734   McIntosh, E.C., Day, J.M.D., Liu, Y., 2018. Insights into Impactor Populations Striking
735   the Moon from Melt Coat and Regolith Meteorite Compositions. Lunar and Planetary
736   Science Conference, 49, 2083.
737   Millet, M.A., Dauphas, N., Greber, N.D., Burton, K.W., Dale, C.W., Debret, B.,
738   Macpherson, C.G., Nowell, G.M., Williams, H.M., 2016. Titanium stable isotope
739   investigation of magmatic processes on the Earth and Moon. Earth and Planetary
740   Science Letters, 449, 197-205.
741   Moynier, F., Albarède, F., Herzog, G.F. 2006. Isotopic composition of zinc, copper, and
742   iron in lunar samples. Geochimica et Cosmochimica Acta 70, 6103–6117.
743   Moynier, F., Agranier, A., Hezel, D.C., Bouvier, A., 2010. Sr stable isotope composition
744   of Earth, the Moon, Mars, Vesta and meteorites. Earth and Planetary Science Letters,
745   300, 359-366.

746   Moynier, F., Vance, D., Fujii, T., Savage, P., 2017. The isotope geochemistry of zinc and
747   copper. Reviews in Mineralogy and Geochemistry, 82, 543-600.
748   Nunes P.D., Tatsumoto M. 1973. Excess lead in "Rusty Rock" 66095 and implications
749   for an early lunar differentiation. Science 182, 916-920.
750   O'Neill, H.S.C., 1991. The origin of the Moon and the early history of the Earth—A
751   chemical model. Part 1: The Moon. Geochimica et Cosmochimica Acta, 55, 1135-
752   1157.
753   Paige, D.A., Siegler, M.A., Zhang, J.A., Hayne, P.O., Foote, E.J., Bennett, K.A.,
754   Vasavada, A.R., Greenhagen, B.T., Schofield, J.T., McCleese, D.J., Foote, M.C.,
755   2010. Diviner lunar radiometer observations of cold traps in the Moon's south polar
756   region. Science, 330, 479-482.
757   Paniello, R.C., Day, J.M.D., Moynier, F. 2012. Zinc isotopic evidence for the origin of
758   the Moon. Nature 490, 376-379.
759   Papanastassiou, D.A., Wasserburg, G.J., Burnett, D.S., 1970. Rb-Sr ages of lunar rocks
760   from the Sea of Tranquillity. Earth and Planetary Science Letters, 8, 1-19.
761   Pieters, C.M., Goswami, J.N., Clark, R.N., Annadurai, M., Boardman, J., Buratti, B.,
762   Combe, J.P., Dyar, M.D., Green, R., Head, J.W., Hibbitts, C., 2009. Character and
763   spatial distribution of OH/H_2O on the surface of the Moon seen by M3 on
764   Chandrayaan-1. Science, 326, 568-572.
765   Poitrasson, F., Halliday, A.N., Lee, D.C., Levasseur, S., Teutsch, N., 2004. Iron isotope
766   differences between Earth, Moon, Mars and Vesta as possible records of contrasted
767   accretion mechanisms. Earth and Planetary Science Letters, 223, 253-266.
768   Poitrasson, F., Delpech, G., Grégoire, M., 2013. On the iron isotope heterogeneity of
769   lithospheric mantle xenoliths: implications for mantle metasomatism, the origin of
770   basalts and the iron isotope composition of the Earth. Contributions to Mineralogy and
771   Petrology, 165, 1243-1258.
772   Polyakov, V.B., Soultanov, D.M., 2011. New data on equilibrium iron isotope
773   fractionation among sulfides: Constraints on mechanisms of sulfide formation in
774   hydrothermal and igneous systems. Geochimica et Cosmochimica Acta, 75, 1957-
775   1974.
776   Pringle, E.A., Moynier, F., 2017. Rubidium isotopic composition of the Earth, meteorites,
777   and the Moon: Evidence for the origin of volatile loss during planetary accretion.
778   Earth and Planetary Science Letters, 473, 62-70.
779   Renggli, C.J., King, P.L., Henley, R.W., Norman, M.D., 2017. Volcanic gas composition,
780   metal dispersion and deposition during explosive volcanic eruptions on the Moon.
781   Geochimica et Cosmochimica Acta, 206, 296-311.
782   Ringwood, A.E., Kesson, S.E., 1977. Basaltic magmatism and the bulk composition of
783   the Moon. The Moon, 16, 425-464.
784   Schultz, P.H., Staid, M.I., Pieters, C.M., 2006. Lunar activity from recent gas release.
785   Nature, 444, 184-187.
786   Scott, S. D., 1983. Chemical behaviour of sphalerite and arsenopyrite in hydrothermal
787   and metamorphic environments. Mineralogical Magazine 47, 427-435.
788   Sedaghatpour, F., Teng, F.Z., Liu, Y., Sears, D.W., Taylor, L.A., 2013. Magnesium
789   isotopic composition of the Moon. Geochimica et Cosmochimica Acta, 120, 1-16.

Sharp, Z.D., Shearer, C.K., McKeegan, K.D., Barnes, J.D., Wang, Y.Q. 2010. The chlorine isotope composition of the Moon and implications for an anhydrous mantle. Science 329, 1050-1053.

Shearer, C.K., Sharp, Z.D., Burger, P.V., McCubbin, F.M., Provencio, P.P., Brearley, A.J., Steele, A. 2014. Chlorine distribution and its isotopic composition in "rusty rock" 66095. Implications for volatile element enrichments of "rusty rock" and lunar soils, origin of "rusty" alteration, and volatile element behavior on the Moon. Geochimica et Cosmochimica Acta 139, 411-433.

Sisson, T.W., Grove, T.L., 1993. Experimental investigations of the role of H_2O in calc-alkaline differentiation and subduction zone magmatism. Contributions to Mineralogy and Petrology, 113, 143-166.

Sossi, P.A., Moynier, F., 2017. Chemical and isotopic kinship of iron in the Earth and Moon deduced from the lunar Mg-suite. Earth and Planetary Science Letters, 471, 125-135.

Sossi, P.A., Halverson, G.P., Nebel, O., Eggins, S.M., 2015. Combined separation of Cu, Fe and Zn from rock matrices and improved analytical protocols for stable isotope determination. Geostandards and Geoanalytical Research, 39, 129-149.

Sossi, P.A., Nebel, O. and Foden, J., 2016. Iron isotope systematics in planetary reservoirs. Earth and Planetary Science Letters, 452, 295-308.

Sossi, P.A., Moynier, F., Van Zuilen, K., 2018. Volatile loss following cooling and accretion of the Moon revealed by chromium isotopes. Proceedings of the National Academy of Sciences, 115, 10920-10925.

Spicuzza M.J., Day J.M.D., Taylor L.A., Valley J.W., 2007. Oxygen isotope constraints on the origin and differentiation of the Moon. Earth and Planetary Science Letters, 253, 254-265.

Syverson, D.D., Luhmann, A.J., Tan, C., Borrok, D.M., Ding, K., Seyfried Jr, W.E., 2017. Fe isotope fractionation between chalcopyrite and dissolved Fe during hydrothermal recrystallization: An experimental study at 350° C and 500 bars. Geochimica et Cosmochimica Acta, 200, 87-109.

Tatsumoto, M., Rosholt, J.N., 1970. Age of the moon: An isotopic study of uranium-thorium-lead systematics of lunar samples. Science, 167, 461-463.

Tatsumoto, M., Premo, W., Unruh, D.M., 1987. Origin of lead from green glass of Apollo 15426: A search for primitive lunar lead. Proc. 17th Lunar Planet. Sci. Conf., JGR 92, E361-E371.

Taylor, L.A., 2012. Water, Water, Everywhere: But How to Find and Use It on the Moon! Annual Meeting of the Lunar Exploration Analysis Group 1685

Taylor L.A., Mao H.K., Bell P.M., 1973. "Rust" in the Apollo 16 rocks. Proc. 4th Lunar Sci. Conf. 829-839.

Taylor, L.A., Mao, H.K., Bell, P.M., 1974. Beta-FeOOH, akaganeite, in lunar rocks. In Lunar and Planetary Science Conference Proceedings, 5, 743-748.

Valdes, M.C., Moreira, M., Foriel, J., Moynier, F., 2014. The nature of Earth's building blocks as revealed by calcium isotopes. Earth and Planetary Science Letters, 394, 135-145.

Walker, R.J., Horan, M.F., Shearer, C.K., Papike, J.J., 2004. Low abundances of highly siderophile elements in the lunar mantle: evidence for prolonged late accretion. Earth and Planetary Science Letters, 224, 399-413.
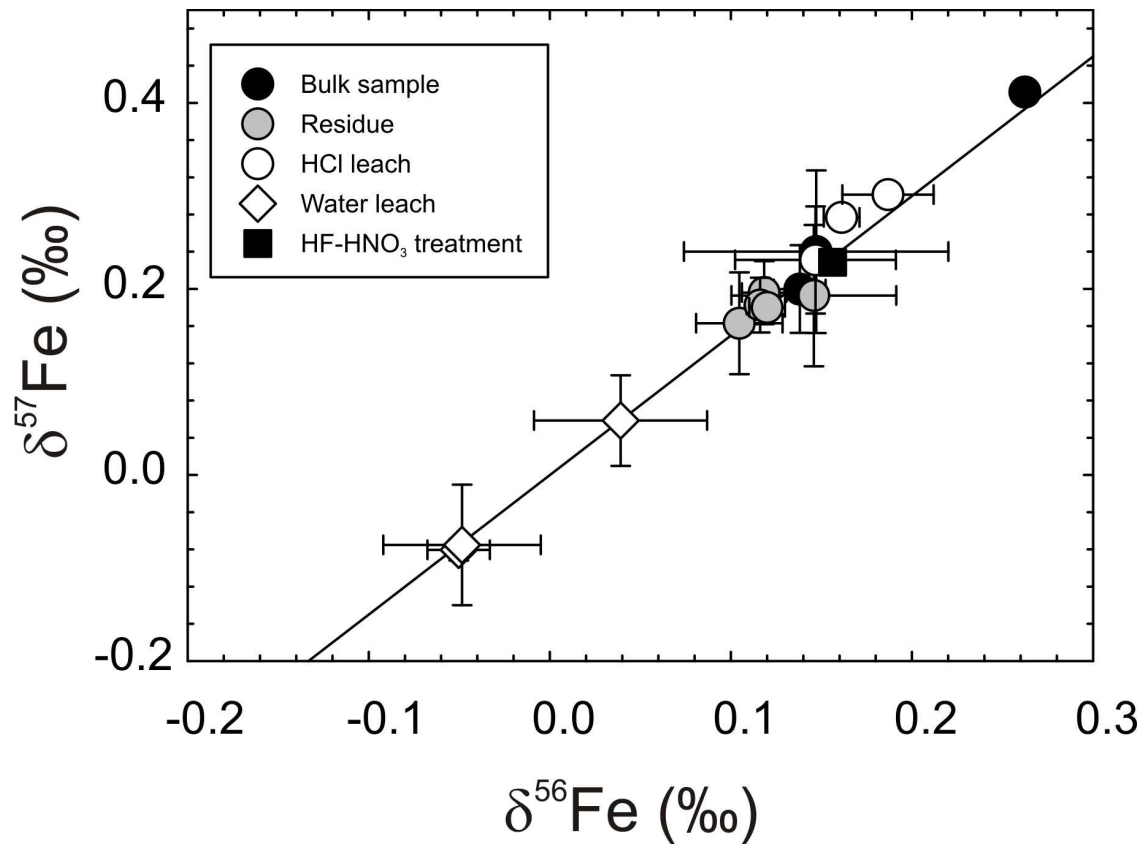
836   Wang, K., Jacobsen, S.B., 2016. Potassium isotopic evidence for a high-energy giant
837   impact origin of the Moon. Nature, 538, 487-490.
838   Wang, K., Moynier, F., Podosek, F.A., Foriel, J., 2012. An iron isotope perspective on
839   the origin of the nanophase metallic iron in lunar regolith. Earth and Planetary Science
840   Letters, 337, 17-24.
841   Wang, K., Jacobsen, S.B., Sedaghatpour, F., Chen, H., Korotev, R.L., 2015. The earliest
842   Lunar Magma Ocean differentiation recorded in Fe isotopes. Earth and Planetary
843   Science Letters, 430, 202-208.
844   Wanke, H., Blum, K., Dreibus, G., Palme, H., Spettel, B., 1981, March. Multielement
845   Analysis of Samples from Highland Breccia 66095: A contribution to the "Rusty
846   Rock" Consortium. Lunar and Planetary Science Conference, 12, 1136-1138.
847   Weyer, S., Anbar, A.D., Brey, G.P., Münker, C., Mezger, K., Woodland, A.B., 2005. Iron
848   isotope fractionation during planetary differentiation. Earth and Planetary Science
849   Letters, 240, 251-264.
850   Wolf, R., Anders, E., 1980. Moon and Earth: compositional differences inferred from
851   siderophiles, volatiles, and alkalis in basalts. Geochimica et Cosmochimica Acta, 44,
852   2111-2124.
853   Young, E.D., Kohl, I.E., Warren, P.H., Rubie, D.C., Jacobson, S.A. and Morbidelli, A.,
854   2016. Oxygen isotopic evidence for vigorous mixing during the Moon-forming giant
855   impact. Science, 351, 493-496.
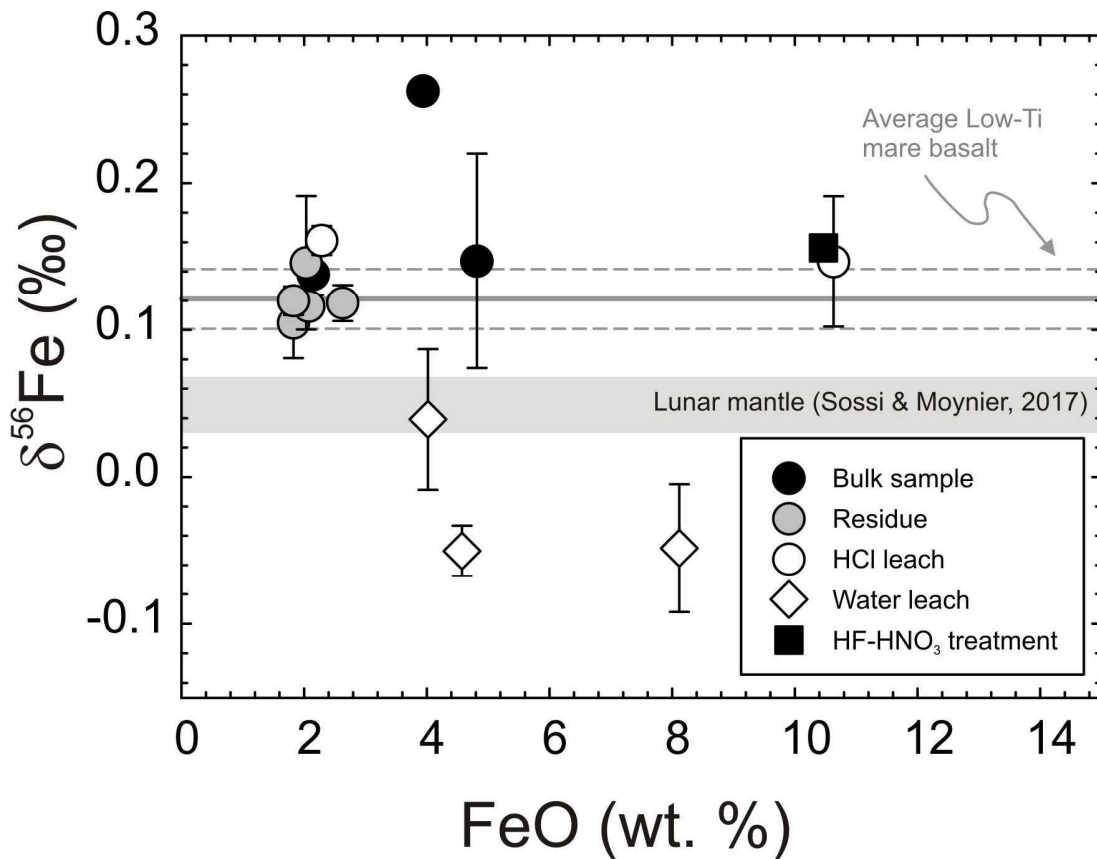
856 **Figures and Figure Captions**
857

858
859
860 **Figure 1:** Copper content versus Cu isotopic composition for compositions measured in
861 66095. Shown is the lunar mare basalt average estimate filtering samples with less than
862 10 µg g^{-1} Cu, from a compilation of published (pub) data from Moynier et al. (2006),
863 Herzog et al. (2009), and Lindsay et al. (2011). PGB are lunar pyroclastic glass beads.

864
865
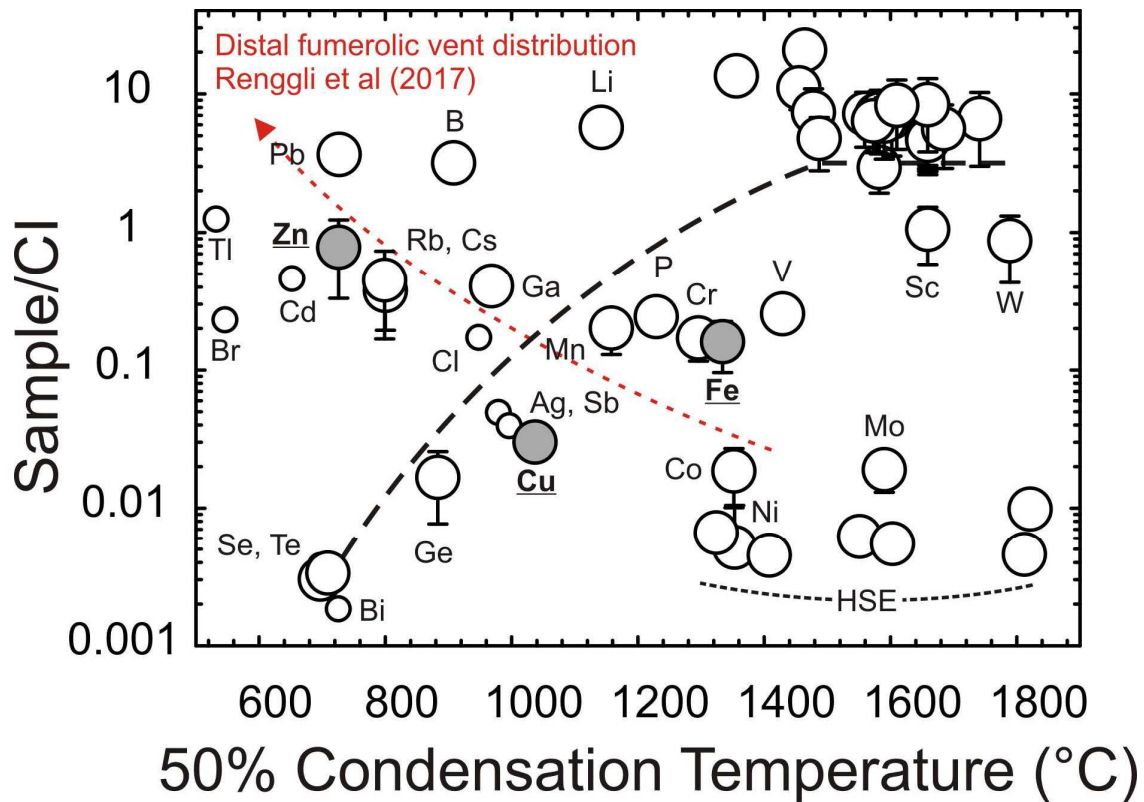866 **Figure 2:** Three-isotope iron plot for compositions measured in 66095. All samples fall
867 on the mass-dependent slope of 1.5.

Figure 4: Plot of 50% Condensation Temperature versus the average compositions of breccia and anorthosite components in 66095, 421, 66095, 425 and 66095, 430 (from Day et al., 2017; large symbols) along with published Tl, Br, Cd, Bi, Cl, Ag and Sb data for 66095 from Krahenbuhl et al. (1973) and Sharp et al. (2010) (smaller symbols), normalized to CI chondrite. Highlighted in 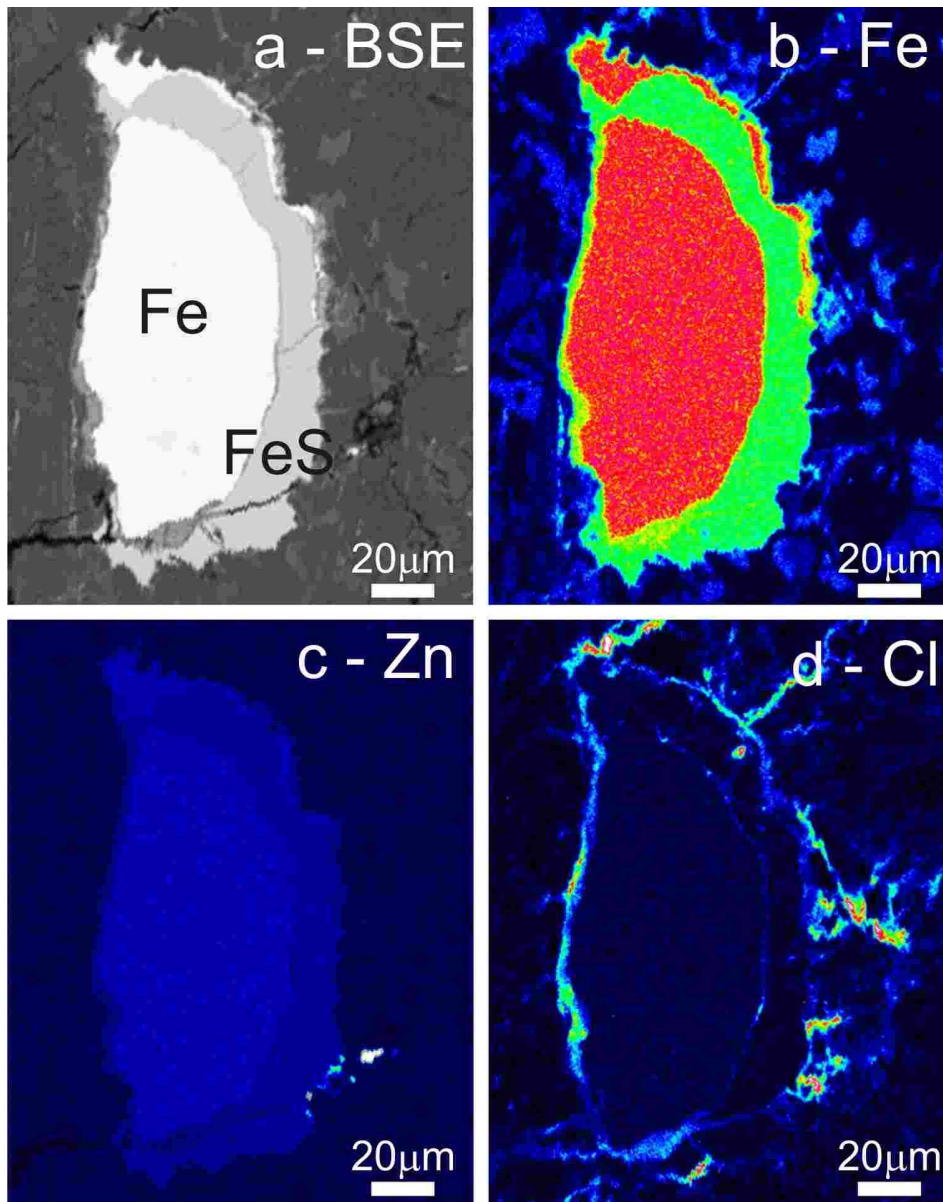grey are the Cu, Fe and Zn abundances. The dashed line is the average lunar volatile depletion trend using data from O'Neill (1991), and red dashed line is the predicted deposition of metals within a lunar fumarolic/volcanic gas distal from the source from Renggli et al. (2017). Condensation temperature values are from Lodders (2003) and CI chondrite normalization is from McDonough & Sun (1995).

887
888
889 **Figure 5:** Location of elements within metal and sulfide grains in the 'Rusty Rock',
890 66095. Warmer and brighter colours correspond to higher concentrations. Iron occurs
891 dominantly within FeNi metal in the sample, whereas Zn is hosted dominantly in
892 sphalerite, and Cl occurs within veins and fractures. (a) Back-Scatter Electron (BSE)
893 image showing primary mineralogy and crystalline texture. Wave-length Dispersive
894 Spectrum (WDS) images of (b) Fe, (c) Zn distribution within sphalerite (bright phase)
895 and (d) Cl distribution within fractures and around metal grains. Fe = metal, FeS =
896 troilite. Image adapted from Day et al. (2017).

Table 1: Iron, copper and zinc isotope data for the 'Rusty Rock' 66095

Sample	Lithology	Type	Experiment	Lab ID	Mass (g)	FeO (wt.%)[a]	FeO (wt.%)	δ^{56}Fe	±2SE	δ^{57}Fe	±2SE	n	Cu μg g^{-1} [a]	Cu μg g^{-1}	δ^{65}Cu	±2SE	n	Zn μg g^{-1}	δ^{66}Zn	±2σ	δ^{67}Zn	±2σ	δ^{68}Zn	±2σ
66095, 421	Breccia	Bulk	Bulk	J1	0.01570	4.5	4.8	0.15	0.07	0.24	0.09	2	3.56	4.71	0.70	0.06	2	102	-13.53	0.05	-20.19	0.11	-26.88	0.10
		Residue (J14)	Exp. 2	J12	0.01340		1.8	0.10	0.02	0.16	0.05	2		18.5	0.72	0.01	2	100	-13.58	0.05	-20.25	0.08	-26.96	0.08
		1M HCl Leach	Exp. 2	J14	0.00900		2.3	0.16	0.01	0.28	0.01	2		2.50	1.38	0.01	2	52.4	-13.27	0.06	-19.81	0.08	-26.34	0.08
		Residue (RR)	Exp. 3	RR1	0.02741		2.6	0.12	0.01	0.20	0.03	2		2.04	0.62	0.03	2	14.8	-13.72	0.03	-20.41	0.06	-27.20	0.06
		20min H$_2$O US	Exp. 3	RR2	0.00064		4.0	0.04	0.05	0.06	0.05	2						395	-8.14	0.31	-12.15	0.42	-16.14	0.65
		20min 3N HCl US	Exp. 3	RR3	0.00610		10.6	0.15	0.04	0.23	0.06	2		7.87	0.70	0.02	2	210	-13.26	0.05	-19.79	0.07	-26.33	0.09
		2hr 1N HF-HNO$_3$	Exp. 3	RR4	0.00482		10.5	0.16	0.01	0.23	0.00	2		11.6	0.63	0.05	2	165	-13.40	0.01	-19.98	0.05	-26.60	0.01
66095, 425 (A)	Anorthosite	Bulk	Bulk	J2	0.00670	2.0	2.2	0.14	0.01	0.20	0.05	2	3.64					397	-13.52	0.07	-20.17	0.10	-26.84	0.13
66095, 425 (B)	Anorthosite	Residue (LP1)	Exp. 1	J3	0.00620	2.4	2.0	0.15	0.05	0.19	0.08	2	3.61	3.23	0.59	0.05	2	325	-13.53	0.03	-20.20	0.06	-26.87	0.06
		30min H$_2$O	Exp. 1	LP1	0.00002		4.6	-0.05	0.02	-0.08	0.01	2						12043	-13.32	0.05	-19.88	0.10	-26.46	0.09
66095, 430	Breccia	Bulk	Bulk	J4	0.00640	5.5	3.9	0.26	0.01	0.41	0.00	2	5.42	6.25	0.79	0.03	2	397	-13.98	0.06	-20.86	0.11	-27.76	0.11
		Residue (LP2)	Exp. 1	J5	0.00980	4.5	2.1	0.12	0.01	0.18	0.03	2	2.90	3.06	0.77	0.07	2	260	-13.02	0.05	-19.40	0.12	-25.83	0.08
		30min H$_2$O	Exp. 1	LP2	0.00003		8.1	-0.05	0.04	-0.08	0.06	2						2577	-12.34	0.04	-18.28	0.07	-24.33	0.04
		Residue (J15)	Exp. 2	J13	0.00770		1.8	0.12	0.01	0.18	0.01	2		4.29	0.59	0.04	2	278	-13.80	0.03	-20.60	0.05	-27.40	0.05
		1M HCl Leach	Exp. 2	J15	0.00013	2.7	24.6	0.19	0.03	0.30	0.00	2	2.71					6709	-13.28	0.05	-19.82	0.07	-26.39	0.08
Milhas Hematite Standard (ETH)								0.51	0.02	0.75	0.02	6												
BHVO-2 (USGS)															0.07	0.06	2							

[a]FeO, Cu and all Zn abundances and isotopic data were previously reported in Day et al. (2017). US = ultra-sonification

Table 2: Mass balance calculations for Fe, Cu and Zn systematics in 66095

Sample	Experiment	Detail	Lab ID	Mass (g)	Fraction	$\sum$FeO (wt.%)	$\sum\delta^{56}$Fe	$\sum$Cu ($\mu g\ g^{-1}$)	$\sum\delta^{65}$Cu	$\sum$Zn ($\mu g\ g^{-1}$)	$\sum\delta^{66}$Zn
66095, 421	Bulk		J1	0.01570	100%	4.82	0.15	4.71	0.70	102.1	-13.5
	Exp. 2	Residue (J14)	J12	0.01340	59.8%	2.01	0.13	12.05	0.98	81.1	-13.5
	Exp. 2	1M HCl Leach	J14	0.00900	40.2%						
	Exp. 3	Residue (RR)	RR1	0.02741	70.3%	4.87	0.13	4.11	0.63	70.1	-13.5
	Exp. 3	20min H_2O US	RR2	0.00064	1.6%						
	Exp. 3	20min 3N HCl US	RR3	0.00610	15.7%						
	Exp. 3	2hr 1N HF-HNO_3	RR4	0.00482	12.4%						
66095, 425 (A)	Bulk		J2	0.00670	100%	2.15	0.14			397.4	-13.5
66095, 425 (B)	Exp. 1	Residue (LP1)	J3	0.00620	99.6%	2.04	0.15	3.23	0.59	366.5	-13.5
	Exp. 1	30min H_2O	LP1	0.00002	0.4%						
66095, 430	Bulk		J4	0.00640	100%	3.94	0.26	6.25	0.79	396.7	-14.0
	Exp. 1	Residue (LP2)	J5	0.00980	99.7%	2.10	0.12	3.06	0.77	267.7	-13.0
	Exp. 1	30min H_2O	LP2	0.00003	0.3%						
	Exp. 2	Residue (J15)	J13	0.00770	98.3%	2.21	0.12	4.21	0.59	384.6	-13.8
	Exp. 2	1M HCl Leach	J15	0.00013	1.7%						

US = ultra-sonification